© 2014. Published by The Company of Biologists Ltd | Development (2014) 141, 2349-2359 doi:10.1242/dev.106633

RESEARCH ARTICLE

TECHNIQUES AND RESOURCES

A microdevice to locally electroporate embryos with high efficiency and reduced cell damage

Elsa Mazari[1], Xuan Zhao[1], Isabelle Migeotte[2], Jérôme Collignon[3], Charlie Gosse[1,*] and Aitana Perea-Gomez[3,*]

ABSTRACT

The ability to follow and modify cell behaviour with accurate spatiotemporal resolution is a prerequisite to study morphogenesis in developing organisms. Electroporation, the delivery of exogenous molecules into targeted cell populations through electric permeation of the plasma membrane, has been used with this aim in different model systems. However, current localised electroporation strategies suffer from insufficient reproducibility and mediocre survival when applied to small and delicate organisms such as early post-implantation mouse embryos. We introduce here a microdevice to achieve localised electroporation with high efficiency and reduced cell damage. *In silico* simulations using a simple electrical model of mouse embryos indicated that a dielectric guide-based design would improve on existing alternatives. Such a device was microfabricated and its capacities tested by targeting the distal visceral endoderm (DVE), a migrating cell population essential for anterior-posterior axis establishment. Transfection was efficiently and reproducibly restricted to fewer than four visceral endoderm cells without compromising cell behaviour and embryo survival. Combining targeted mosaic expression of fluorescent markers with live imaging in transgenic embryos revealed that, like leading DVE cells, non-leading ones send long basal projections and intercalate during their migration. Finally, we show that the use of our microsystem can be extended to a variety of embryological contexts, from preimplantation stages to organ explants. Hence, we have experimentally validated an approach delivering a tailor-made tool for the study of morphogenesis in the mouse embryo. Furthermore, we have delineated a comprehensive strategy for the development of ad hoc electroporation devices.

KEY WORDS: Localised electroporation, Mouse embryo, Microsystem, Visceral endoderm, Migration, Organ explant, Finite element model simulations

INTRODUCTION

During embryonic development, morphogenesis is the result of dynamic and complex cellular events controlled by signalling networks finely regulated in space and time. Understanding these processes requires the ability to label discrete cell populations in order to characterise their lineage and fate and to modify gene expression with precise spatiotemporal resolution.

Electroporation consists in delivering exogenous molecules into cells via the electric permeabilisation of the plasma membrane. It has been widely used to introduce nucleic acids in model organisms (Calegari et al., 2004; Escoffre et al., 2009; Nakamura and Funahashi, 2012; Swartz et al., 2001). Unlike viral infection and lipofection, electroporation does not require specific sample preparation. Moreover, spatial and temporal control of gene expression is achieved without the obligatory identification of tissue-specific regulatory sequences, nor the time- and resource-consuming production of genetically modified animals.

Targeting electroporation to specific tissues often involves local application of the exogenous molecule and generation of an electric field with large electrodes, either commercially available or home-made. This approach has been implemented most successfully when the tissue of interest surrounds a natural body cavity in which microinjection is possible, for example the neural tube lumen or the proamniotic cavity of vertebrate embryos (Itasaki et al., 1999; Soares et al., 2008). In other situations, such as experiments involving epithelial tissues lying at the periphery of embryos or organs, the geometry and the position of the targeted area do not allow local concentration of the exogenous molecule. The latter compound is then homogeneously distributed, and localised electroporation can only be achieved if the electric field is spatially restricted, for instance by using needle-shaped electrodes placed close to the targeted area (Davidson et al., 2003; Momose et al., 1999). The main limitation of this strategy is that electrolysis at the surface of the needles leads to pH variations and gas bubble generation that can be detrimental to the adjacent cells (Kim et al., 2008; Wang et al., 2010; Wang and Lee, 2013). This problem can be circumvented by relying on electrodes placed at a distance from the organism while channelling the electric field through narrow dielectric guides filled with an electrolyte, a technique notably applied to label single neurons with electroporation micropipettes (Haas et al., 2001; Nolkrantz et al., 2001; Wang et al., 2010). Recently, dielectric guide-based electroporation has also been adapted to the on-chip format, with microfabricated electrodes and fluidic channels (Fox et al., 2006; Wang et al., 2010; Wang and Lee, 2013). Although the use of such devices has so far been restricted to single cells in culture, one could in principle devise similar microsystems to target small embryos or organ explants that face poor survival in traditional electroporation experiments. This is the case for mouse embryos at early post-implantation stages, a crucial time-window for anterior-posterior axis formation (Rossant and Tam, 2009; Takaoka and Hamada, 2012).

Shortly after implantation, at embryonic day 5 of development (E5), the mouse embryo has the shape of an elongated cylinder, less than 200 µm long, and displays radial symmetry around the proximo-distal axis. The pluripotent epiblast (Epi) in the distal region is associated to two extra-embryonic tissues, the extra-embryonic ectoderm (ExE), which abuts the epiblast proximally, and the visceral endoderm (VE), an absorptive epithelium essential for nutrient exchange that forms the outer layer of the conceptus. Dynamic reciprocal signalling between the epiblast and the extra-embryonic tissues results in radial symmetry

[1]Laboratoire de Photonique et de Nanostructures, LPN-CNRS, route de Nozay, 91460 Marcoussis, France. [2]Institut de Recherche Interdisciplinaire en Biologie Humaine et Moléculaire, Université Libre de Bruxelles, Brussels 1070, Belgium. [3]Institut Jacques Monod, CNRS, UMR7592, Univ Paris Diderot, Sorbonne Paris Cité, F-75205 Paris, France.

*Authors for correspondence (charlie.gosse@lpn.cnrs.fr; pereagomez.aitana@ijm.univ-paris-diderot.fr)

Received 2 December 2013; Accepted 8 April 2014

Development (2014) 141, 2349-2359 doi:10.1242/dev.106633

breaking, specification of the anterior-posterior axis, gastrulation initiation, and formation of the definitive germ layers. Central to these processes is a VE subpopulation identified at E5.5 by a specific morphology and the expression of a distinct gene repertoire: the distal visceral endoderm (DVE). These cells will move proximally towards one side of the embryo, where they will define the future anterior pole and hence take the name of anterior visceral endoderm (AVE) at E6.5 (Rossant and Tam, 2009; Takaoka and Hamada, 2012).

DVE migration has been followed by live imaging of transgenic embryos where this cell population is selectively marked by the expression of fluorescent proteins, e.g. Hex-GFP (Rodriguez et al., 2001). This approach has demonstrated that DVE cells migrate while keeping epithelial integrity by intercalating between other VE cells (Migeotte et al., 2010; Srinivas et al., 2004; Trichas et al., 2011, 2012). Moreover, cell tracking has shown that the whole VE layer is involved in a global reorganisation initiated by DVE motion (Rivera-Perez et al., 2003; Takaoka et al., 2011; Trichas et al., 2011). Detailed observation of DVE cells at the migration front revealed that they send long actin-dependent projections, which possibly sense the environment for orientation cues (Migeotte et al., 2010; Srinivas et al., 2004). Ablation experiments during the initial phase of migration indicated that front row cells act as leading cells and are essential for subsequent movements in the VE (Morris et al., 2012; Takaoka et al., 2011). By contrast, it has been difficult to scrutinise the shape and behaviour of DVE cells located in the midst of the migrating fluorescent population or of other non-labelled VE cells. It is thus currently unknown whether they also send long extensions and intercalate or whether they are dragged by the leading DVE cells. Answering these questions requires new tools to specifically target chosen populations and create cell mosaics in the VE layer.

We here describe an on-chip approach based on dielectric guides that makes localised electroporation efficient, reproducible and safe. As a proof of principle, we have chosen to target small cell populations in the VE of mouse embryos at E5.5-E6.5, a crucial stage for which existing electroporation procedures face poor reproducibility and poor embryo survival. By combining our new electroporation strategy with live imaging in transgenic embryos, we provide evidence that, during anterior-posterior axis formation, active migration and intercalation are not restricted to leading DVE cells. Finally, we demonstrate that the microdevice we designed can be used to electroporate tissues in a wide range of embryonic contexts.

RESULTS

Numerical simulations validate a design based on dielectric guides to locally permeate the outer epithelium of embryos

Electroporation of early post-implantation mouse embryos has first been achieved in a chamber with parallel plate electrodes (Fig. 1B) (Mellitzer et al., 2002; Soares et al., 2008). However, it can be inferred from computations of the electric potential at the surface of an ellipsoid model that although permeation localisation is optimal when the longer axis of the embryo is perpendicular to both electrodes, it degrades as soon as a tilt angle exists, becoming nearly impossible after a 90° rotation (Valic et al., 2003). This limitation has been overcome by replacing one of the plates by a needle (Fig. 1C), thereby creating a significant variation of the electric potential over a small area (Davidson et al., 2003; Khoo et al., 2007). Importantly, permeation is efficiently restricted in space only if the needle is close enough to the targeted tissue, which may result in cell damage. To circumvent this problem, we considered a third approach where the electric field generated by large electrodes is conveyed to the targeted zone by dielectric guides (Fig. 1D) (Wang et al., 2010; Wang and Lee, 2013).

In order to compare the three strategies, a simple electrical model of the embryo was conceived (Fig. 1A) and numerical simulations were undertaken to evaluate the extent of membrane permeation for each setup. It was here assumed that exogenous molecules could enter the cells of the outer epithelium only if the absolute value of the induced transmembrane voltage (ITV) exceeded a given threshold (Escoffre et al., 2009; Rols and Teissie, 1998). To determine the latter parameter, the ITV value on the anterior surface of E6.5 embryos was first plotted in the dielectric guide case

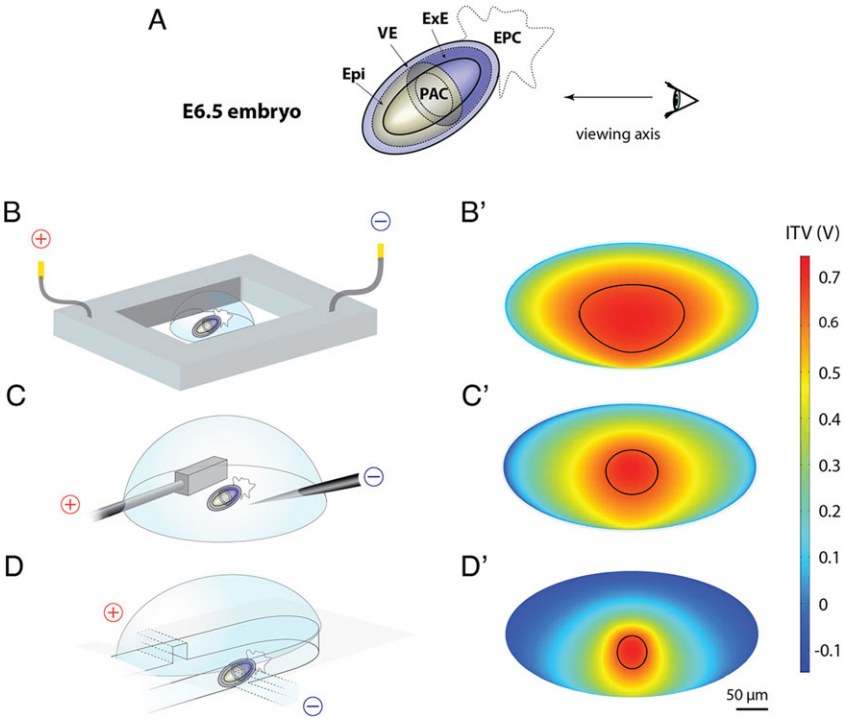

Fig. 1. Numerical simulations for the electroporation of the outer epithelial cells located on the anterior half of E6.5 embryos. (A) The embryo is approximated by two concentric prolate ellipsoids of respective length and width 400 and 200 µm for the buffer/VE interface and 300 and 100 µm for the PAC/Epi+ExE one (dimensions established according to our observations, Fig. 3A,C,D and Fig. 4A). Solid lines depict those two liquid/tissue interfaces, whereas dashed lines represent tissue/tissue junctions not considered in computations. Techniques relying on (B,B′) parallel plate electrodes, (C,C′) plate and needle electrodes and (D,D′) 110×60 µm^2 dielectric guides are compared. The geometries used to simulate the experimental situations schematised in B, C and D are detailed in supplementary material Fig. S2. B′,C′ and D′ display the ITV on flattened views of the anterior half of E6.5 embryos, using 34, 2 and 15 V pulse amplitudes, respectively. The same 0.72 V maximal ITV value is then reached in all three cases. Black lines delimitate the areas where the ITV is superior to the 0.65 V permeation threshold. Epi, epiblast; EPC, ectoplacental cone; ExE, extra-embryonic ectoderm; PAC, proamniotic cavity; VE, visceral endoderm.

Development (2014) 141, 2349-2359 doi:10.1242/dev.106633

(Fig. 1D′) and the results of these computations were analysed with respect to experimental data on FITC-Dextran incorporation. As measurements provided an electroporated length corresponding to 8% of the total proximo-distal length (see below, Fig. 4A), the permeation threshold was fixed at 0.65 V in order to achieve consistency. Incidentally, this value is within the range of those reported for isolated cells (Escoffre et al., 2009; Hibino et al., 1993; Valic et al., 2003; Wang et al., 2010). Next, the parallel plates and the plate and needle setups were simulated. The pulse amplitudes were chosen to yield ITV maxima identical to the 0.72 V obtained with the dielectric guides, thereby allowing the comparison of the three approaches. When targeting the AVE at E6.5 with parallel plate electrodes, up to 14% of the embryo anterior half displayed an ITV beyond the permeation threshold (Fig. 1B′). The extent of the electroporated area was reduced to 4% when using the plate and needle electrodes (Fig. 1C′), and further decreased to 2% with the dielectric guides (Fig. 1D′).

Keeping the same permeation threshold, similar conclusions were reached when targeting the DVE at E5.5: parallel plate electrodes, plate and needle electrodes, and dielectric guides respectively yielded electroporation of 7%, 4% and 2% of the embryo distal half (supplementary material Fig. S1).

Microfabrication techniques enable to easily and reproducibly fabricate dielectric guides

Both the single-use SU-8/Parafilm devices and the subsequent reusable glass/Parafilm ones were designed following a similar layout (Fig. 2A,B; supplementary material Figs S5 and S7). A keyhole-shaped open chamber at the centre enables easy embryo manipulation. At both extremities, large electrodes are located at the bottom of open circular reservoirs that allow the evacuation of gas bubbles produced by electrolysis, thus preventing these insulating objects from disrupting current flow and hindering membrane permeation. Each reservoir is connected to the chamber by a fluidic system including a narrow dielectric guide and a wider connecting channel. The shape of the aperture in front of which the embryo is placed is the most important parameter affecting electroporation localisation. Geometry was here adjusted to the size of the developing organism (Fig. 2C-F). On the other hand, the dielectric guide length was set so as to achieve ITV in the order of 0.5 to 1 V while applying voltage pulses with amplitudes remaining in the electroporator working range, i.e. 10 to 90 V.

Materials were first selected according to considerations related to microfabrication: glass is cheap and widely used in microfluidics; SU-8 is a well-known high-aspect-ratio epoxy-photoresist that allows features up to 200 µm high; Parafilm is easy to pattern with cutters and punchers, it can also be straightforwardly bonded under moderate heating. Regarding biocompatibility, SU-8 and gold were favoured as their innocuousness has been demonstrated for numerous cell and tissue types (Ereifej et al., 2011; Kotzar et al., 2002).

Dielectric guide-based devices allow efficient electroporation with reduced cell damage

Validation of the design and functionality of our chip was performed by electroporating the VE of E6.5 and E5.5 mouse embryos. Efficient membrane permeabilisation was assessed by FITC-Dextran penetration (Fig. 3A,F). Cell transfection by nucleic acids was evaluated through the expression of fluorescent proteins 24 h after electroporation of plasmids encoding Venus or mCherry (Fig. 3B,G). Finally, electrically induced cell damage was asserted when at least one cell displayed PI incorporation shortly after pulse

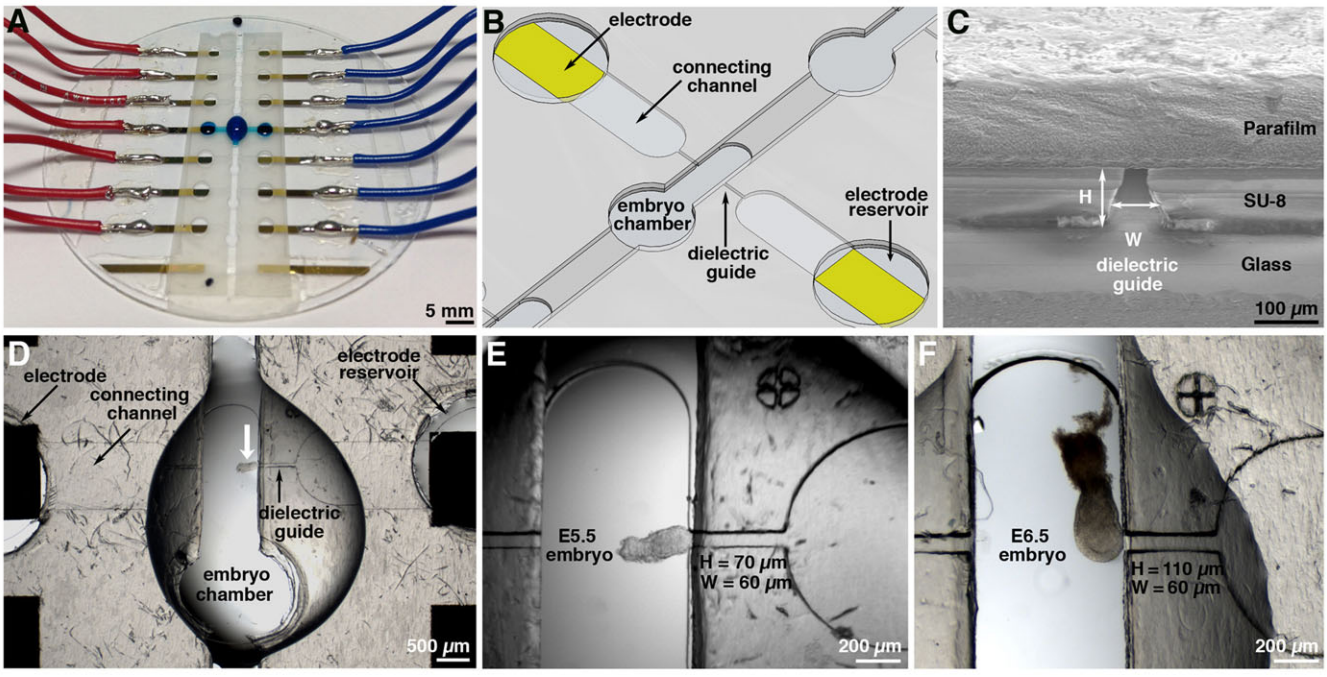

Fig. 2. Layout and use of the dielectric guide-based electroporation device. (A) Global view of the microsystem, one of the fluidic networks being filled with a Bromophenol Blue solution to highlight connectivity. (B) Diagram showing a pair of electrodes with the corresponding connecting channels, dielectric guides and embryo chamber. (C) Scanning electron microscopy micrograph of a dielectric guide of height H=110 µm and width W=60 µm, as observed from the embryo chamber. (D) View of the whole fluidic system included between the electrodes. An E5.5 embryo (white arrow) is positioned so as to target its DVE, this tissue facing the dielectric guide connected to the cathode. (E) Zoom on the E5.5 embryo. (F) Similar enlarged view of an E6.5 embryo positioned so as to target its AVE.

Development (2014) 141, 2349-2359 doi:10.1242/dev.106633

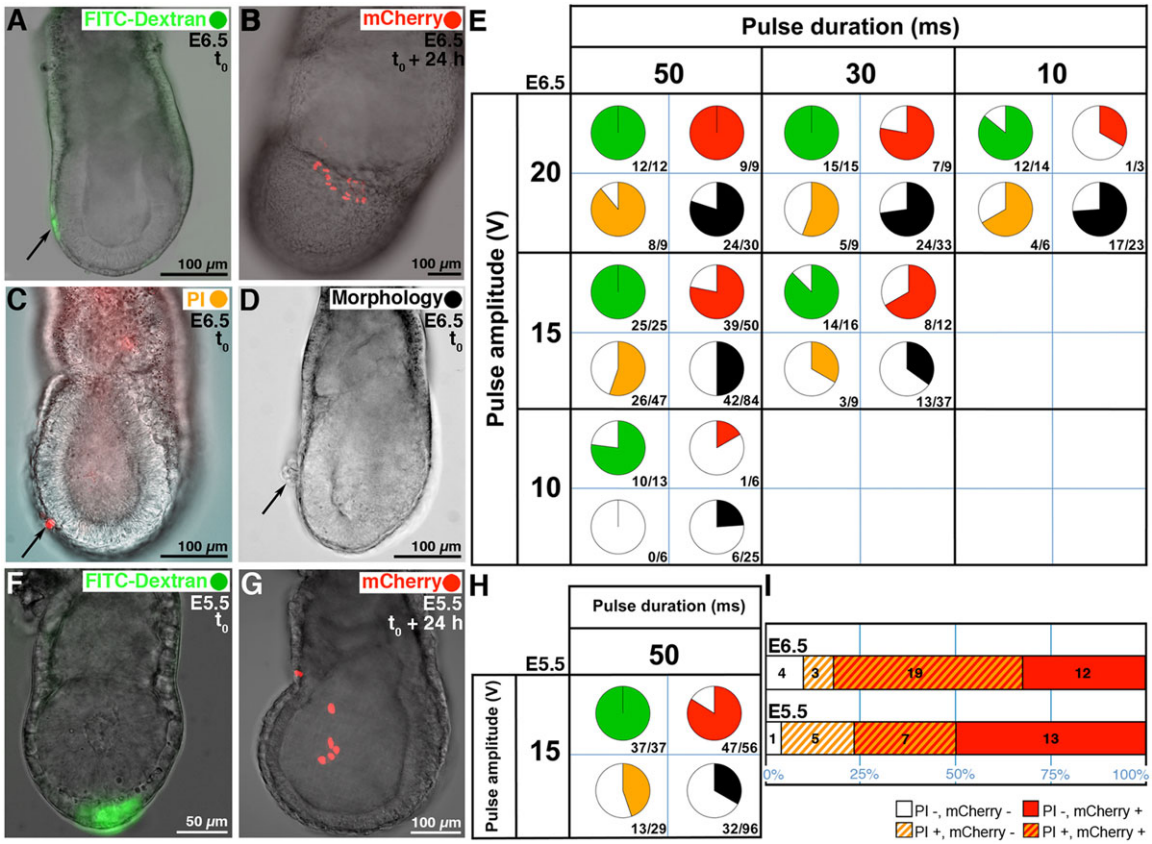

Fig. 3. Electroporation outcome for E6.5 and E5.5 embryos submitted to a series of three identical square voltage pulses of various amplitude and duration, and separated by 1 s. Representative examples for the criteria used to define electrical conditions suitable to electroporate AVE cells at E6.5: (A) FITC-Dextran incorporation (black arrow); (B) nuclear mCherry expression; (C) PI incorporation (black arrow); (D) abnormal morphology such as cell swelling or destruction (black arrow). (E) Results for E6.5 embryos electroporated using 110×60 µm^2 dielectric guides. Coloured sectors report on the percentage of embryos in which at least one cell of the VE displays the following characteristics: (green) FITC-Dextran incorporation; (red) Venus or mCherry expression; (orange) PI incorporation; (black) abnormal morphology. The *p*/*n* fraction indicated below each pie chart corresponds to the number of positive results, *p*, over the total number of electroporated embryos, *n*. Representative examples for the criteria used to define electrical conditions suitable to electroporate DVE cells at E5.5: (F) FITC-Dextran incorporation; (G) nuclear mCherry expression. (H) Results for E5.5 embryos electroporated using 70×60 µm^2 dielectric guides. (I) Analysis of the co-appearance in single embryos of cell death (PI incorporation) and efficient transfection (mCherry expression) after electroporation with 15 V and 50 ms pulses at E6.5 (*n*=38) and E5.5 (*n*=26). Anterior is to the left in A-D and G.

application (Fig. 3C). Distinct batches of embryos were used to score these three outputs, whereas morphological alterations were monitored for all groups (Fig. 3D).

E6.5 embryos, early to mid-streak stage, were electroporated with their AVE facing a 110 µm high and 60 µm wide dielectric guide (Fig. 2F), using a range of electrical conditions close to those predicted by numerical simulations (Fig. 3E). Efficient pore opening occurred in all cases as revealed by FITC-Dextran incorporation. Moreover, embryo survival was not impaired as 100% of the electroporated embryos reached the late bud to head fold stage after 24 h of *in vitro* culture, irrespective of the presence of local cell damages (*n*=232, Fig. 3E). For 20 V pulses, local cell death was induced in the majority of the embryos as evidenced by PI incorporation. Reducing pulse duration at this voltage did not improve cell viability while DNA transfection was dramatically reduced, an effect likely to be due to insufficient electrophoretical transport of the plasmids to the permeabilised membrane (Escoffre et al., 2009; Rols and Teissie, 1998). By contrast, 10 V pulses preserved cell viability but failed to trigger transfection. Applying three pulses of 15 V, 50 or 30 ms long and spaced by 1 s yielded high transfection efficiency and good cell viability. These conditions were also optimal for the electroporation of DVE cells at E5.5 (Fig. 3F-H; data not shown), with the height of the dielectric guides being reduced to 70 µm, so as to maintain localisation in these smaller organisms (Fig. 2E).

The co-appearance of efficient DNA transfection and cell damage in individual embryos was next analysed for electroporation with the 15 V and 50 ms conditions. The percentage of embryos expressing mCherry that showed no cell death was 39% and 65% at E6.5 and E5.5, respectively (Fig. 3I; supplementary material Figs S8 and S9). For both stages, DNA transfection and PI incorporation were independent events (Fisher's exact test, two-tailed, P=0.42 and P=0.07, Fig. 3I). PI incorporation strongly correlated to the appearance of morphological abnormalities upon pulse application (supplementary material Figs S8 and S9), indicating that visual scoring alone can allow the identification of embryos with irreversible local cell damage.

Dielectric guide-based devices allow reproducible localised electroporation

Two approaches were undertaken to address the size of the electroporated area with the previously established 15 V and 50 ms conditions. First, the length of the zone showing FITC-Dextran fluorescence along the proximo-distal axis was measured in a subset of E6.5 embryos shortly after electroporation (Fig. 4A). The signal extended over 33±7 µm (*n*=13), representing 3-4 cell

Development (2014) 141, 2349-2359 doi:10.1242/dev.106633

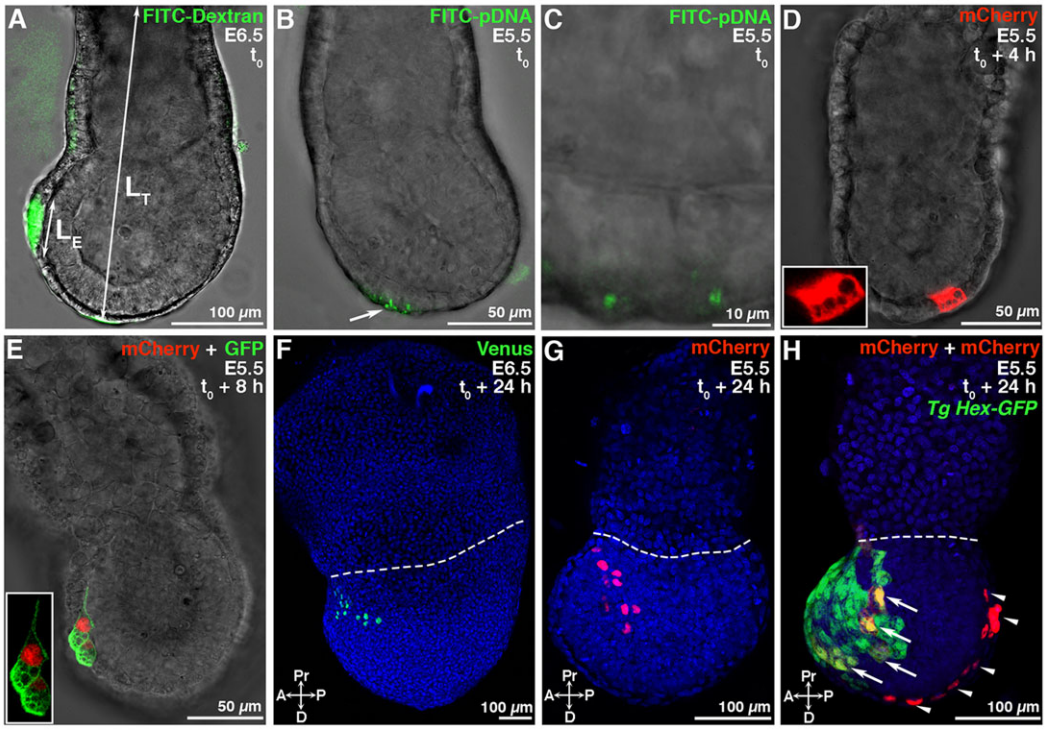

Fig. 4. Localised VE electroporation of E6.5 and E5.5 embryos with 15 V and 50 ms pulses, using 110×60 μm^2 and 70×60 μm^2 dielectric guides, respectively. (A) FITC-Dextran incorporation after AVE electroporation at E6.5. The fluorescent signal extends over a length L_E, and the total embryo length L_T is measured from the basis of the ectoplacental cone to the distal tip. (B) FITC-labelled pCAG-nls-mCherry plasmid interacting with the plasma membrane 45 min after DVE electroporation at E5.5. Superposition of the maximum intensity projection of a confocal stack comprising 19 slices spaced by 2 μm and of a single transmission plane. (C) Single plane view of the region indicated by the white arrow in B. (D) Cytoplasmic mCherry expression 4 h after DVE electroporation at E5.5. Single confocal plane. (E) Fluorescent protein expression targeted to the nucleus and to the plasma membrane 8 h after co-electroporation of pCAG-nls-mCherry and pCMV-GAP43myr-EGFP in the DVE at E5.5. Single confocal plane. (F) Nuclear Venus distribution 24 h after AVE electroporation at E6.5. Maximum intensity projection of a confocal stack comprising 81 slices spaced by 3 μm. (G) Nuclear mCherry distribution 24 h after DVE electroporation at E5.5. Maximum intensity projection of a confocal stack comprising 29 slices spaced by 5 μm. (H) Cytoplasmic (arrows) and nuclear (arrowheads) mCherry expression 24 h after double electroporation of pCAG-mCherry and pCAG-nls-mCherry, respectively, in the DVE and in the posterior visceral endoderm of a E5.5 Hex-GFP transgenic embryo. Maximum intensity projection of a confocal stack comprising 34 slices spaced by 5 μm. Inserts show close up views in D,E. Hoechst-stained nuclei are shown in blue and white dashed lines highlight the embryonic/extra-embryonic boundary in F-H. A, anterior; D, distal; P, posterior; Pr, proximal.

diameters and 8±2% of the total embryo length. Second, FITC or Cy3-labelled plasmids were used to electroporate the DVE at E5.5. These molecules were visible as spots at the surface of the targeted cells just after pulse application and up to 4 h later (Fig. 4B,C). Such fluorescent spots have previously been observed when electroporating isolated cells and probably correspond to plasmids that form a stable complex with the plasma membrane before being internalised into the cytoplasm (Escoffre et al., 2009; Golzio et al., 2002). Confocal imaging indicated that in all cases four cells were marked under these conditions (n=6, Fig. 4B,C).

Fluorescent protein expression was detected in one to four VE cells 4 h after plasmid electroporation (Fig. 4D, n=14), a timing in agreement with previous observations (Davidson et al., 2003; Khoo et al., 2007). Prominent apical vacuoles and basal projections in migrating DVE cells were observed when cytoplasmic or membrane-targeted fluorescent proteins were used (Fig. 4D,E; supplementary material Movie 1), indicating that transfected cells show similar characteristics to unmanipulated ones (Migeotte et al., 2010; Rivera-Perez et al., 2003; Srinivas et al., 2004; Wada et al., 2013).

After 24 h of whole embryo culture, the spatial distribution of the fluorescent cells was consistent with the morphogenetic displacements reported for each subpopulation. AVE cells targeted at E6.5 were found at proximal anterior positions (Fig. 4F). For E5.5 embryos, labelled DVE cells had migrated anteriorly and laterally (Fig. 4G,H), whereas electroporated posterior visceral endoderm cells were found at posterior and distal positions (Fig. 4H) (Lawson and Pedersen, 1987; Perea-Gomez et al., 2001; Rivera-Perez et al., 2003; Srinivas et al., 2004; Takaoka et al., 2011). Transfection of E6.5 AVE and E5.5 DVE respectively yielded 12±7 and 9±5 fluorescent cells after 24 h (n=14 and n=26, respectively). These results are compatible with a VE population doubling time previously estimated to 10-12 h by clonal analysis (Lawson and Pedersen, 1987; Perea-Gomez et al., 2001).

Localised electroporation reveals the behaviour of VE cells in the mouse embryo

The analysis of transgenic embryos in which DVE cells specifically express a fluorescent protein has shed light on the behaviour of cells at the migration front. However, these studies only dealt with the initial phase of DVE movement and did not address in detail the characteristics of DVE cells located in the midst of the GFP-expressing population, where the outlines of individual cells could not be distinguished (Migeotte et al., 2010; Srinivas et al., 2004; Takaoka et al., 2011; Trichas et al., 2011). We combined localised electroporation, transgenic lines and live imaging to tackle this question.

E5.5-5.75 Hex-GFP transgenic embryos were electroporated distally with a plasmid encoding cytoplasmic mCherry and imaged by live confocal microscopy from 10 to 20 h after electroporation (Fig. 5; supplementary material Movies 2 and 3). All embryos

Development (2014) 141, 2349-2359 doi:10.1242/dev.106633

developed normally (n=5), as assessed by the stereotyped anterior and lateral movement of Hex-GFP expressing cells. When electroporated cells divided, they did so only once during the 10 h imaging, in line with the cell cycle length in the VE at this stage. In all cases, divisions were characterised by rounding of cells and mitosis was completed in less than 30 min (n=9 divisions observed in three embryos, Fig. 5B-C″). Moreover, nearby labelled cells divided synchronously, indicating some degree of coordination in clonally related neighbours (Fig. 5B″-C″).

We focused our analysis on the behaviour of electroporated cells found in the anterior region of the VE, once the Hex-GFP positive migration front had reached the embryonic/extra-embryonic (Emb-Xemb) border (Fig. 5; supplementary material Movies 2 and 3). The anterior VE comprises Hex-GFP-positive and Hex-GFP-negative cellular clusters (Migeotte et al., 2010; Srinivas et al., 2004) and we could target both populations. Labelled cells expressing mCherry showed a net distal to proximal displacement corresponding to 2 to 4 cell diameters (38±16 µm, displacement of n=5 cells measured in two embryos) during the 10 h culture period (Fig. 5; supplementary material Movies 2 and 3). This observation is in agreement with the finding that VE cells in the anterior region continue to undergo a proximal movement after leading DVE cells have reached the Emb-Xemb border at E5.75 (Takaoka et al., 2011).

Prominent basal projections were observed for both Hex-GFP-positive and -negative mCherry-expressing cells as they moved forward and intercalated (Fig. 5). These projections were oriented towards the proximal region, had an average length of 13±7 µm, and lasted from 15 min to 1.5 h (n=30 measurements performed on 11 cells in the embryos shown in Fig. 5; supplementary material Movies 2 and 3). The longer, up to 30 µm, and more stable projections were observed in cells reaching the proximity of the Emb-Xemb border. Thin extensions, longer than two cell diameters, appeared to contact the first or second row of Hex-GFP positive cells in the proximal region, through filopodial-like tips (Fig. 5E,E″,F,F″; supplementary material Movies 2 and 3).

Previous studies had shown that after the initial phase of migration, DVE cells make an abrupt halt when they reach the Emb-Xemb border, become elongated with their long axis parallel to the border and spread on the anterior surface of the embryo (Migeotte et al., 2010; Srinivas et al., 2004; Trichas et al., 2011). We

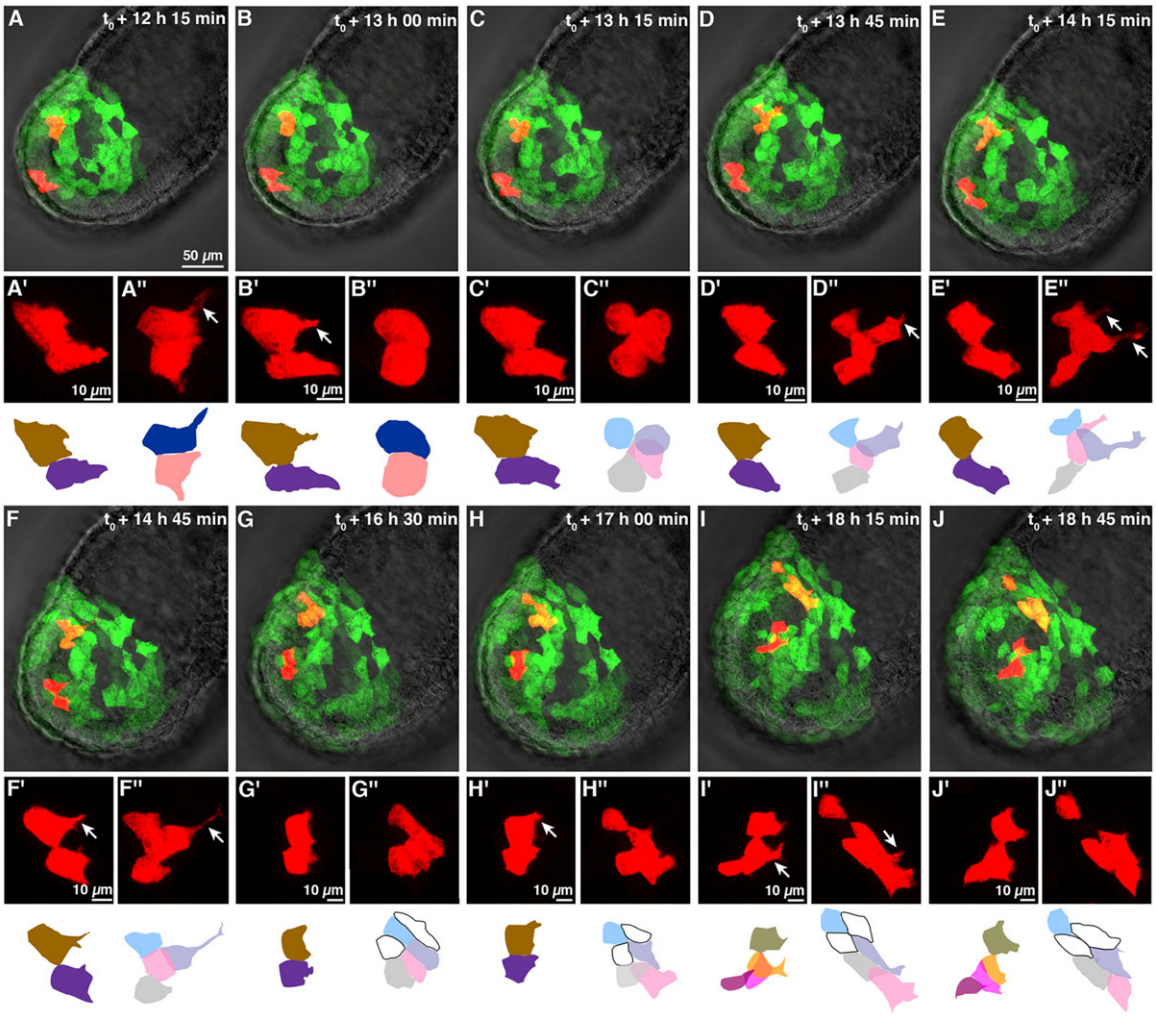

Fig. 5. Confocal live imaging of a Hex-GFP E5.5 embryo electroporated in the VE with pCAG-mCherry with 15 V and 50 ms pulses, using 70×60 µm^2 dielectric guides. Images were acquired every 15 min for 10 h. (A-J) Superpositions of a single transmission plane with the maximum intensity projection of mCherry and GFP fluorescence from a stack comprising 25 slices spaced by 4 µm. (A′-J″) Close-up fluorescence views at each time point of the distal Hex-GFP negative (A′-J′) and proximal Hex-GFP positive (A″-J″) mCherry-expressing cells. White arrows show cell projections. Maximal intensity projections and individual confocal sections were used to draw diagrams where the electroporated cells are coloured and the outlines of some of the Hex-GFP expressing cells are shown in black.

Development (2014) 141, 2349-2359 doi:10.1242/dev.106633

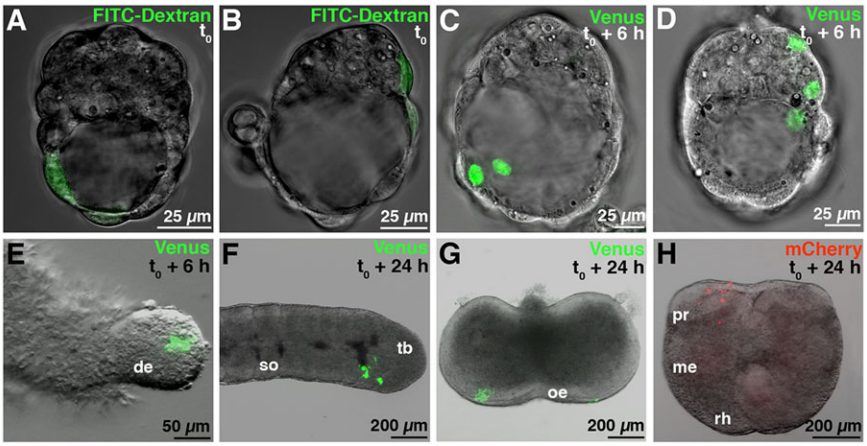

Fig. 6. Electroporation of E3.5 blastocysts and organ explants with 20 V and 50 ms pulses, using 60×50 μm² and 110×60 μm² dielectric guides, respectively. In E3.5 blastocysts, FITC-Dextran incorporation (A,B) and nuclear Venus expression (C,D) in mural (A,C) and polar (B,D) trophectoderm. In organ explants, nuclear Venus expression after electroporation of an E11.5 lung endodermal bud explant (E), an E11.5 tail bud explant (F), and an E9.5 mandibular arch explant (G). (H) Nuclear mCherry expression after electroporation of an E8.5 anterior neural plate explant. de, distal endoderm; me, mesencephalon; oe, oral epithelium; pr, prosencephalon; rh, rhombencephalon; so, somite; tb, tail bud.

observed that non-leading Hex-GFP-positive cells also ceased forward movement and adopted elongated shapes, but they did so before reaching the Emb-Xemb border, stopping just distally to the first rows of leading Hex-GFP-positive cells (Fig. 5G-J″; supplementary material Movie 2). In addition, lateral spreading of the non-leading cells also involved intercalation and junction remodelling (Fig. 5G-J″).

Dielectric guide-based devices allow the localised electroporation of external epithelia in embryos and explants

By adapting the dimensions of the dielectric guides, smaller or larger samples could also be targeted with the new microsystem. E3.5 blastocysts were electroporated using 60 μm high and 50 μm wide guides, and upon appropriate orientation mural or polar trophectoderm were always selectively labelled with FITC-Dextran (n=9, Fig. 6A,B). Venus expression was observed in 83% of the cases 6 h after electroporation (positive embryos/analysed embryos, p/n=10/12, 3±1 labelled cells, Fig. 6C,D; supplementary material Movie 4). By using dielectric guides 110 μm high and 60 μm wide, localised electroporation was successfully achieved in several organ explants: E11.5 lung endoderm buds (Fig. 6E, p/n=8/8), E11.5 tail buds (Fig. 6F, p/n=10/10), E9.5 mandibular arches (Fig. 6G, p/n=6/6) and E8.5 anterior neural plates (Fig. 6H, p/n=4/6).

Dielectric guide-based devices fabricated in glass can be reused

The above results demonstrate that the proposed microsystem design allows an efficient and reproducible localised electroporation. During performance optimisation, which was achieved by sequential improvements of prototypes, we favoured ease of fabrication over robustness. Indeed, the microfluidic network was patterned in SU-8, a material difficult to clean and regenerate after use. In order to overcome this limitation, an alternative glass-based fabrication protocol was implemented (Fig. 7A,B; supplementary material Figs S6 and S7). Despite some differences in the geometry due to the use of a wet etching technique, a comparable design yielded similar electroporation results when E5.5 DVE cells were targeted. All the electroporated embryos reached the early streak stage after one day of *in vitro* culture (n=20). Localised FITC-Dextran incorporation was each time successful (n=11, Fig. 7C). Upon plasmid electroporation, 67% of the embryos expressed nuclear Venus and showed 9±2 fluorescent cells after 18 to 20 h in culture (p/n=6/9, Fig. 7D). Importantly, no difference in results was noticed when the glass wafer was reused after being cleaned.

DISCUSSION

We have produced a chip to locally electroporate small embryos and explants in an efficient, reproducible and safe way. Although the advantages of miniaturisation have been widely recognised when dealing with single cells (Boukany et al., 2011; Fox et al., 2006; Wang et al., 2010; Wang and Lee, 2013), microfabrication techniques have only rarely been adopted for the electroporation of developing organisms (Bansal et al., 2009; Huang et al., 2007). To our knowledge this work validates for the first time the superiority of dielectric guide based designs when targeting small cell populations in embryos. When applied to early post-implantation stages in mouse, our microsystem offers important benefits over the approaches relying on plate and/or needle electrodes (Davidson et al., 2003; Khoo et al., 2007): embryo survival is always assured and small populations of fewer than four cells can be transfected without noticeable modification of their behaviour. Moreover, immobilisation of the sample by suction in front of the dielectric guide and targeting of one or more selected regions can be performed under a conventional dissecting microscope with no need for micromanipulation, unlike in the lipofection or microinjection approaches (Lawson and Pedersen, 1987; Yamamoto et al., 2004).

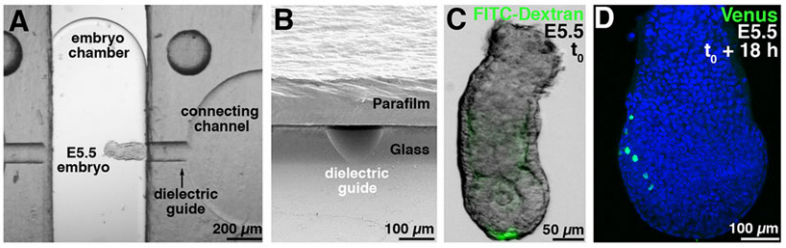

Fig. 7. Electroporation experiments performed with the reusable glass microdevice, using 15 V and 50 ms pulses. (A) Close-up view of a chip with an E5.5 embryo positioned so as to target its DVE. (B) Scanning electron microscopy micrograph of a dielectric guide of height H=70 μm, as observed from the embryo chamber. (C) Example of an E5.5 embryo showing FITC-Dextran incorporation in the DVE. (D) Nuclear Venus distribution 18 h after electroporation. Superposition of the maximum intensity projection of a confocal stack comprising 56 slices spaced by 3 μm. Anterior is to the left in D. Hoechst-stained nuclei are shown in blue.

Development (2014) 141, 2349-2359 doi:10.1242/dev.106633

Combining localised electroporation with the use of transgenic mouse lines and live imaging revealed new behaviours of VE cells during anterior-posterior axis formation. Previous studies had reported that DVE cells at the migration front are required to initiate DVE movement, therefore acting as a leading population (Morris et al., 2012; Takaoka et al., 2011). Their displacement involves intercalation and production of long and stable basal projections (Migeotte et al., 2010; Srinivas et al., 2004). Our results show that non-leading DVE cells behave similarly, indicating that they are not passively dragged and that they potentially sense cues to regulate their progression. In addition, upon reaching the proximity of the Emb/Xemb border, non-leading DVE cells extend very long projections that appear to contact the first or second cell rows of the migration front. It is tempting to speculate that distally located Emb VE cells need to make contact with the subpopulation of leading DVE cells, which is characterised by a distinct origin and specific expression of the markers Cer1 and Lefty1 (Morris et al., 2012; Takaoka et al., 2011), in order to receive the signals that regulate their migration and/or arrest.

The optimisation process leading to the design of the new electroporation microsystem first involved soft-lithography (Mazari et al., 2011) before a fabrication protocol based on the SU-8 photoresist could yield effective prototypes. However, at this stage, chips remained single-use. In order to make our transfection technique accessible to a wide community of users, we have developed, as an intermediate milestone, a reusable hybrid device composed of a removable Parafilm lid and of a glass wafer in which the dielectric guides have been etched. The latter part, the sole including features realised thanks to microtechnologies, can be recycled through washing and hydrophilisation procedures easy to perform on any wet bench. Future work will aim at obtaining a complete glass-based chip, for which no assembly will be necessary and only simple cleaning will be required before use.

The present comprehensive strategy coupling numerical simulations, prototype microfabrication and *in vivo* testing, provides a framework that will be helpful for the realisation of electroporation devices tailor-made for a variety of samples: whole embryos from different species, e.g. *Xenopus* (Chernet and Levin, 2012; Falk et al., 2007), chick (Nakamura et al., 2004; Voiculescu et al., 2008), zebrafish (Bansal et al., 2009; Huang et al., 2007), insects (Ando and Fujiwara, 2013); organ explants, e.g. brain (Barker et al., 2009; del Rio and Soriano, 2010), retina (Matsuda and Cepko, 2004), cochlea (Driver and Kelley, 2010), gut (Abud et al., 2008), gonads (Gao et al., 2011); or *in vitro* reconstituted tissues, e.g. spheroids (Chopinet et al., 2011; Mellor et al., 2006). Here, by adjusting the dimensions of the dielectric guides, the microsystem dedicated to early post-implantation mouse embryos was straightforwardly adapted to blastocysts and mouse embryonic organ explants, which had different sizes and shapes. Future implementations at either smaller or larger scales can thus easily be foreseen (Bansal et al., 2009; Boukany et al., 2011; Falk et al., 2007; Voiculescu et al., 2008). Likewise, the size of the targeted region can be modulated by modifying the dielectric guide cross-section. Finally, in the present design efficient electric field focusing ensures excellent electroporation localisation for external tissues. However, our localisation strategy cannot be applied to internal tissues, located further away from the dielectric guides. Our preliminary results issued from numerical simulations indicate that the pulse amplitude required to reach the permeabilisation threshold for inner cells would be deleterious for outer ones (data not shown). Combining local injection of DNA with the use of very large dielectric apertures (Falk et al., 2007), or relying on more invasive guides to penetrate the internal tissue and reach the targeted area (Haas et al., 2001; Nolkrantz et al., 2001), would provide alternative approaches to circumvent this problem.

A variety of molecules can be efficiently introduced into cells by electroporation, including DNA, mRNA (Cerda et al., 2006; Chernet and Levin, 2012), dsRNA (Mellitzer et al., 2002; Soares et al., 2008), morpholinos (Falk et al., 2007; Mellitzer et al., 2002; Voiculescu et al., 2008), siRNA (Calegari et al., 2004; Paganin-Gioanni et al., 2011), proteins (Rols et al., 1998; Rols and Teissie, 1998) and drugs (Teissie et al., 2012). In this work we concentrated on DNA electroporation to provide a readout for transfection. Incidentally, we confirmed for the first time in a live organism the formation of transient DNA aggregates at the plasma membrane. This observation highlights the interest of coupling our safe electroporation protocol with live imaging to investigate the mechanistic aspects of DNA electrotransfer in complex *in vivo* environments, such as the ones faced in clinical applications of electromediated nucleic acid delivery (Andre and Mir, 2010; Chabot et al., 2013; Mir et al., 1999; Rols et al., 1998).

Finally, associating efficient localised electroporation with the rapidly evolving fluorescent protein-based tools for optogenetics (Nowotschin and Hadjantonakis, 2009; Tang et al., 2013; Yin and Wu, 2013) will surely provide new powerful approaches for the investigation of the cellular bases of morphogenesis.

MATERIALS AND METHODS

Numerical simulations

In order to evaluate which cells are permeated upon voltage application we built simplified models of experimental situations (Fig. 1; supplementary material Figs S1-S3) and used the Comsol Multiphysics 4.2a software (Comsol) to compute the electric potential both outside and inside the embryo. The ITV at the VE surface was calculated by subtracting the extracellular potential at the embryo periphery to its cytoplasmic counterpart (Fig. 1; supplementary material Fig. S1). Each time this parameter exceeded a given threshold, pores were assumed to form (Escoffre et al., 2009; Rols and Teissie, 1998). Incidentally, the contribution of the resting potential to the total transmembrane voltage was neglected because its −20 to −60 mV value (Valic et al., 2003; Wang et al., 2010) was smaller than the incertitude evaluated for threshold determination.

Early post-implantation embryos were modelled as two concentric prolate ellipsoids, the outer one representing the organism external boundary and the inner one the periphery of the proamniotic cavity (Fig. 1; supplementary material Fig. S1). Cells were not considered individually, as they are electrically connected by GAP junctions (Pucihar et al., 2009), present in all tissues at these developmental stages (Kalimi and Lo, 1988; Viotti et al., 2012). No data being available for the electrical properties of mouse embryos, values reported for various cell types were used (Gowrishankar and Weaver, 2003; Hibino et al., 1993; Pucihar et al., 2006; Sudsiri et al., 2007). The two ellipsoids were described as resistive membranes having a 3×10^{-7} S/m conductivity and a 5 nm thickness. The conductivity of the proamniotic fluid was assumed identical to that of the cytoplasm and fixed at 0.3 S/m. For the electroporation buffer a 1.5 S/m value was measured using a CDM210 conductimeter (Radiometer analytical). The glass, polymer and air boundaries were insulating. The cathode surface was grounded and the anode one had its potential corresponding to the pulse amplitude.

Microfabrication

Devices were realized in the LPN clean room using standard microfabrication techniques (Abgrall and Gue, 2007). An abbreviated version of these lengthy processes is given below, and the detailed procedures and dimensions can be found in supplementary material Figs S4-S7.

The single-use SU-8/Parafilm chips were produced on D263 glass substrates, 50 mm in diameter and 550 µm thick (Opticad) (Fig. 2; supplementary material Fig. S4). Gold thin-film electrodes, spaced by 5.8 mm, were first obtained using a lift-off procedure. Then, the walls of the 650 µm wide embryo chamber and of the 415 µm long dielectric guides

Development (2014) 141, 2349-2359 doi:10.1242/dev.106633

were patterned in SU-8 2050 (MicroChem). The thickness H of the epoxy-resist layer and the width W of the dielectric guides were adjusted to the size of the electroporated organism, varying from 60 to 110 µm and from 50 to 60 µm, respectively (supplementary material Fig. S5). Next, the polymer surface was hydrophilised by plasma treatment. Finally, the fluidic system was closed by thermal bonding of a 130 µm thick ceiling made of Parafilm 'M' (Pechiney) including the necessary access holes.

For fabrication of the reusable glass/Parafilm device (Fig. 7; supplementary material Figs S6 and S7) a chromium mask was first patterned on the D263 substrate by optical lithography followed by ion beam etching. Hydrofluoric acid was subsequently used to selectively etch the fluidic network in the wafer bulk up to H=70 µm, which resulted in guides with a rounder profile. After electrodes were deposited, the glass surface was hydrophilised in a basic solution. Finally, the Parafilm lid was assembled. Following electroporation, glass substrate recycling was performed by peeling off the Parafilm, cleaning the organic traces in trichloroethylene and the mineral ones in a caustic soda solution. A new surface activation and the bonding of a new lid could then be undertaken.

Mouse strains, embryo collection, *in vitro* culture of whole embryos and explants

Embryos were obtained from natural matings of wild-type Swiss females with either Swiss males or transgenic Hex-GFP males maintained on a mixed C57Bl/6 CBA/J and Swiss background (embryos obtained from males of the C57Bl/6 CBA/J background alone were less resistant to the electroporation procedure, data not shown). E5.5 and E6.5 embryos were dissected in DMEM, 10% fetal calf serum, 25 mM Hepes buffer pH 7.0 (Gibco) and cultured at 37°C and 5% CO_2 in, respectively, 50% or 75% heat-inactivated rat serum in DMEM/F12, 100 µg/ml streptomycin, 100 U/ml penicillin, by groups of three in 200 µl or individually in 30 µl. E3.5 blastocysts were flushed from uterine horns in M2 medium (Sigma), depellucidated in acid Tyrode's solution, and cultured in 10 µl of G2 medium (Vitrolife) covered with mineral oil. E11.5 lung endodermal bud explants, obtained after removal of mesenchyme with pancreatin/trypsin treatment, were cultured in Matrigel (Becton Dickinson) (Weaver et al., 2000). E11.5 tail buds, E9.5 mandibular arches, and E8.5 anterior neural plate explants were cultured on Millicell organotypic inserts (Millipore) (Chai et al., 1998; Shimamura and Rubenstein, 1997). Experiments were performed in accordance with French Agricultural Ministry and European guidelines for the care and use of laboratory animals (certificate CEB-35-2012 delivered by ethical committee CEEA-40).

Markers for electroporation

Fluorescein-labelled dextran (FITC-Dextran, 4 kDa, Sigma) was dissolved at 2 mg/ml in HBS (150 mM NaCl, 20 mM Hepes buffer pH 7.0). pCAG-mCherry, pCAG-nls-mCherry, pCMV-GAP43myr-EGFP (the myristoylation sequence of GAP43 targets EGFP to the plasma membrane), and pCAG-nls-Venus endotoxin-free plasmids were diluted at 1 to 1.5 µg/µl in HBS. Concentrations were selected according to literature (Davidson et al., 2003; Khoo et al., 2007; Rols and Teissie, 1998). For immediate visualisation of DNA electroporation, plasmids were labelled with either Cy3 or fluorescein using the Label IT Tracker kit (Mirus) (Boukany et al., 2011). Incubating the embryos in FITC-Dextran or in fluorescently labelled plasmid solutions for 5 min did not result in any fluorescence above background (data not shown), ruling out any significant endocytic uptake of these markers by VE cells during the procedure. Furthermore, marker molecular weights above 1 kDa precluded diffusion from cell to cell through GAP junctions (Kalimi and Lo, 1988).

Electroporation protocols

For each electroporation, 15 µl of solution containing the exogenous molecule were applied to the device, starting with the electrode reservoirs to easily achieve dielectric guide filling. Individual embryos or explants were briefly rinsed in HBS and transferred to the central chamber, with the targeted area facing the cathodic channel (Fig. 2D-F). A small residual flow, probably due to pressure differences between droplets of different volumes in the electrode reservoirs and the embryo chamber, kept the organism steady in front of the guide opening during the procedure (2 to 3 min per sample). A train of three square pulses of duration 10 to 50 ms and amplitude 10 to 20 V, spaced by 1 s, was immediately applied using a TSS20 Ovodyne electroporator (Intracel).

When addressing cell death, electroporated embryos were cultured for 30 min and stained for 20 min at 37°C in dissection medium containing 25 µg/ml of propidium iodide (PI, Sigma). PI staining did not modify the efficiency of transfection with plasmid DNA. Control embryos submitted to the whole protocol with the exception of pulse application did not show any PI incorporation (data not shown).

Wide-field and confocal microscopy

To document FITC-Dextran and PI incorporation, embryos were imaged 1 to 3 h after electroporation using a DMI6000B inverted microscope (Leica) equipped with 20×/0.7NA and 10×/0.4NA lenses. For detailed investigations on the position and number of electroporated cells, embryos were fixed in PBS/paraformaldehyde 4% at 4°C for 1 h and stained with 10 µg/ml Hoechst 33342 (Molecular Probes). Confocal images were obtained using a LSM 710 confocal microscope (Zeiss) equipped with 25×/0.8NA and 40×/1.3NA lenses.

Time-lapse microscopy

Individual E5.5 electroporated embryos were transferred into wells of angiogenesis µ-slides (Ibidi) containing 30 µl of culture medium and imaged for up to 16 h on an inverted LSM 710 confocal microscope (Zeiss) equipped with a 40×/1.3NA lens. Cell projections were measured on 3D images by manually selecting their tip and basis and using the 'Filament tracer' function of Imaris 7.6.4 (Bitplane).

Acknowledgements

We are indebted to the staff of the LPN clean room, the ImagoSeine platform, and the IJM animal facility for excellent technical assistance. We thank L. Couraud, C. Dupuis and L. Leroy for performing metallization and electron microscopy, A.-C. Louër and W. Supatto for useful discussions, C. Papanayotou and S. Meilhac for gifts of plasmids, G. Duval for help with embryo culture, G. Dubois, J. Laniel, M. Mantelet and J. Iranzo for participating in initial experiments, A. Camus, H. Berthoumieux, C. Papanayotou, P.-H. Puech and D. Sabéran-Djoneidi for critical reading of the manuscript.

Competing interests

The authors declare no competing financial interests.

Author contributions

A.P.-G. and C.G. conceived and coordinated the project; E.M. and C.G. performed numerical simulations; C.G., E.M. and X.Z. designed and fabricated electroporation devices; A.P.-G. and E.M. carried out electroporations and analysed data with contributions of I.M.; A.P.-G. and C.G. wrote the manuscript with contributions of E.M., I.M., X.Z. and J.C.

Funding

This work was supported by ElectroMice, Biomodulator and ElectroTagMan grants from the Centre National de la Recherche Scientifique (CNRS) PI 2008, Agence Nationale de la Recherche (ANR) PNANO 2009, and C'nano IdF 2011 calls, respectively. E.M. was the recipient of PhD scholarships from the Fondation pour la Recherche Médicale (FRM) and from the Réseau Thématique de Recherche Avancée (RTRA) 'Triangle de la Physique' (ElectroMagSign project). I.M. is a research associate of the Fonds National de la Recherche Scientifique (FNRS).

Supplementary material

Supplementary material available online at
http://dev.biologists.org/lookup/suppl/doi:10.1242/dev.106633/-/DC1

References

Abgrall, P. and Gué, A.-M. (2007). Lab-on-chip technologies: making a microfluidic network and coupling it into a complete microsystem – a review. *J. Micromech. Microeng.* **17**, R15-R49.

Abud, H. E., Young, H. M. and Newgreen, D. F. (2008). Analysing tissue and gene function in intestinal organ culture. *Methods Mol. Biol.* **468**, 275-286.

Ando, T. and Fujiwara, H. (2013). Electroporation-mediated somatic transgenesis for rapid functional analysis in insects. *Development* **140**, 454-458.

Andre, F. M. and Mir, L. M. (2010). Nucleic acids electrotransfer in vivo: mechanisms and practical aspects. *Curr. Gene Ther.* **10**, 267-280.

Bansal, T., Lenhart, J., Kim, T., Duan, C. and Maharbiz, M. M. (2009). Patterned delivery and expression of gene constructs into zebrafish embryos using microfabricated interfaces. *Biomed. Microdevices* **11**, 633-641.

Development (2014) 141, 2349-2359 doi:10.1242/dev.106633

Barker, M., Billups, B. and Hamann, M. (2009). Focal macromolecule delivery in neuronal tissue using simultaneous pressure ejection and local electroporation. *J. Neurosci. Methods* **177**, 273-284.

Boukany, P. E., Morss, A., Liao, W.-C., Henslee, B., Jung, H., Zhang, X., Yu, B., Wang, X., Wu, Y., Li, L. et al. (2011). Nanochannel electroporation delivers precise amounts of biomolecules into living cells. *Nat. Nanotechnol.* **6**, 747-754.

Calegari, F., Marzesco, A.-M., Kittler, R., Buchholz, F. and Huttner, W. B. (2004). Tissue-specific RNA interference in post-implantation mouse embryos using directional electroporation and whole embryo culture. *Differentiation* **72**, 92-102.

Cerda, G. A., Thomas, J. E., Allende, M. L., Karlstrom, R. O. and Palma, V. (2006). Electroporation of DNA, RNA, and morpholinos into zebrafish embryos. *Methods* **39**, 207-211.

Chabot, S., Rosazza, C., Golzio, M., Zumbusch, A., Teissie, J. and Rols, M.-P. (2013). Nucleic acids electro-transfer: from bench to bedside. *Curr. Drug Metab.* **14**, 300-308.

Chai, Y., Bringas, P., Jr, Shuler, C., Devaney, E., Grosschedl, R. and Slavkin, H. C. (1998). A mouse mandibular culture model permits the study of neural crest cell migration and tooth development. *Int. J. Dev. Biol.* **42**, 87-94.

Chernet, B. T. and Levin, M. (2012). A versatile protocol for mRNA electroporation of Xenopus laevis embryos. *Cold Spring Harb. Protoc.* **2012**, 447-452.

Chopinet, L., Wasungu, L. and Rols, M.-P. (2011). First explanations for differences in electrotransfection efficiency in vitro and in vivo using spheroid model. *Int. J. Pharm.* **423**, 7-15.

Davidson, B. P., Tsang, T. E., Khoo, P.-L., Gad, J. M. and Tam, P. P. L. (2003). Introduction of cell markers into germ layer tissues of the mouse gastrula by whole embryo electroporation. *Genesis* **35**, 57-62.

del Río, J. A. and Soriano, E. (2010). Regenerating cortical connections in a dish: the entorhino-hippocampal organotypic slice co-culture as tool for pharmacological screening of molecules promoting axon regeneration. *Nat. Protoc.* **5**, 217-226.

Driver, E. C. and Kelley, M. W. (2010). Transfection of mouse cochlear explants by electroporation. *Curr. Protoc. Neurosci.* Chapter 4, Unit 4 34 1-10.

Ereifej, E. S., Khan, S., Newaz, G., Zhang, J., Auner, G. W. and VandeVord, P. J. (2011). Characterization of astrocyte reactivity and gene expression on biomaterials for neural electrodes. *J. Biomed. Mater. Res. A* **99A**, 141-150.

Escoffre, J.-M., Portet, T., Wasungu, L., Teissié, J., Dean, D. and Rols, M.-P. (2009). What is (still not) known of the mechanism by which electroporation mediates gene transfer and expression in cells and tissues. *Mol. Biotechnol.* **41**, 286-295.

Falk, J., Drinjakovic, J., Leung, K. M., Dwivedy, A., Regan, A. G., Piper, M. and Holt, C. E. (2007). Electroporation of cDNA/Morpholinos to targeted areas of embryonic CNS in Xenopus. *BMC Dev. Biol.* **7**, 107.

Fox, M. B., Esveld, D. C., Valero, A., Luttge, R., Mastwijk, H. C., Bartels, P. V., van den Berg, A. and Boom, R. M. (2006). Electroporation of cells in microfluidic devices: a review. *Anal. Bioanal. Chem.* **385**, 474-485.

Gao, L., Kim, Y., Kim, B., Lofgren, S. M., Schultz-Norton, J. R., Nardulli, A. M., Heckert, L. L. and Jorgensen, J. S. (2011). Two regions within the proximal steroidogenic factor 1 promoter drive somatic cell-specific activity in developing gonads of the female mouse. *Biol. Reprod.* **84**, 422-434.

Golzio, M., Teissie, J. and Rols, M.-P. (2002). Direct visualization at the single-cell level of electrically mediated gene delivery. *Proc. Natl. Acad. Sci. U.S.A.* **99**, 1292-1297.

Gowrishankar, T. R. and Weaver, J. C. (2003). An approach to electrical modeling of single and multiple cells. *Proc. Natl. Acad. Sci. U.S.A.* **100**, 3203-3208.

Haas, K., Sin, W.-C., Javaherian, A., Li, Z. and Cline, H. T. (2001). Single-cell electroporation for gene transfer in vivo. *Neuron* **29**, 583-591.

Hibino, M., Itoh, H. and Kinosita, K., Jr. (1993). Time courses of cell electroporation as revealed by submicrosecond imaging of transmembrane potential. *Biophys. J.* **64**, 1789-1800.

Huang, K.-S., Lin, Y.-C., Su, K.-C. and Chen, H.-Y. (2007). An electroporation microchip system for the transfection of zebrafish embryos using quantum dots and GFP genes for evaluation. *Biomed. Microdevices* **9**, 761-768.

Itasaki, N., Bel-Vialar, S. and Krumlauf, R. (1999). 'Shocking' developments in chick embryology: electroporation and in ovo gene expression. *Nat. Cell Biol.* **1**, E203-E207.

Kalimi, G. H. and Lo, C. W. (1988). Communication compartments in the gastrulating mouse embryo. *J. Cell Biol.* **107**, 241-255.

Khoo, P. L., Franklin, V. J. and Tam, P. P. (2007). Fate-mapping technique: targeted whole-embryo electroporation of DNA constructs into the germ layers of mouse embryos 7-7.5 days post-coitum. *CSH Protoc.* **2007**, pdb prot4893.

Kim, J. A., Cho, K., Shin, M. S., Lee, W. G., Jung, N., Chung, C. and Chang, J. K. (2008). A novel electroporation method using a capillary and wire-type electrode. *Biosens. Bioelectron.* **23**, 1353-1360.

Kotzar, G., Freas, M., Abel, P., Fleischman, A., Roy, S., Zorman, C., Moran, J. M. and Melzak, J. (2002). Evaluation of MEMS materials of construction for implantable medical devices. *Biomaterials* **23**, 2737-2750.

Lawson, K. A. and Pedersen, R. A. (1987). Cell fate, morphogenetic movement and population kinetics of embryonic endoderm at the time of germ layer formation in the mouse. *Development* **101**, 627-652.

Matsuda, T. and Cepko, C. L. (2004). Electroporation and RNA interference in the rodent retina in vivo and in vitro. *Proc. Natl. Acad. Sci. U.S.A.* **101**, 16-22.

Mazari, E., Mantelet, M., Iranzo, J., Perea-Gomez, A. and Gosse, C. (2011). Localized electroporation of mouse embryo using dielectric guides. Transducers 2011, Digest of the Technical Papers of the 16th International Conference on Solid-State Sensors, Actuators, and Microsystems, 1172-1175.

Mellitzer, G., Hallonet, M., Chen, L. and Ang, S.-L. (2002). Spatial and temporal 'knock down' of gene expression by electroporation of double-stranded RNA and morpholinos into early postimplantation mouse embryos. *Mech. Dev.* **118**, 57-63.

Mellor, H. R., Davies, L. A., Caspar, H., Pringle, C. R., Hyde, S. C., Gill, D. R. and Callaghan, R. (2006). Optimising non-viral gene delivery in a tumour spheroid model. *J. Gene Med.* **8**, 1160-1170.

Migeotte, I., Omelchenko, T., Hall, A. and Anderson, K. V. (2010). Rac1-dependent collective cell migration is required for specification of the anterior-posterior body axis of the mouse. *PLoS Biol.* **8**, e1000442.

Mir, L. M., Bureau, M. F., Gehl, J., Rangara, R., Rouy, D., Caillaud, J.-M., Delaere, P., Branellec, D., Schwartz, B. and Scherman, D. (1999). High-efficiency gene transfer into skeletal muscle mediated by electric pulses. *Proc. Natl. Acad. Sci. U.S.A.* **96**, 4262-4267.

Momose, T., Tonegawa, A., Takeuchi, J., Ogawa, H., Umesono, K. and Yasuda, K. (1999). Efficient targeting of gene expression in chick embryos by microelectroporation. *Dev. Growth Differ.* **41**, 335-344.

Morris, S. A., Grewal, S., Barrios, F., Patankar, S. N., Strauss, B., Buttery, L., Alexander, M., Shakesheff, K. M. and Zernicka-Goetz, M. (2012). Dynamics of anterior-posterior axis formation in the developing mouse embryo. *Nat. Commun.* **3**, 673.

Nakamura, H. and Funahashi, J. (2012). Electroporation: past, present and future. *Dev. Growth Differ.* **55**, 15-19.

Nakamura, H., Katahira, T., Sato, T., Watanabe, Y. and Funahashi, J. (2004). Gain- and loss-of-function in chick embryos by electroporation. *Mech. Dev.* **121**, 1137-1143.

Nolkrantz, K., Farre, C., Brederlau, A., Karlsson, R. I. D., Brennan, C., Eriksson, P. S., Weber, S. G., Sandberg, M. and Orwar, O. (2001). Electroporation of single cells and tissues with an electrolyte-filled capillary. *Anal. Chem.* **73**, 4469-4477.

Nowotschin, S. and Hadjantonakis, A.-K. (2009). Photomodulatable fluorescent proteins for imaging cell dynamics and cell fate. *Organogenesis* **5**, 217-226.

Paganin-Gioanni, A., Bellard, E., Escoffre, J. M., Rols, M. P., Teissie, J. and Golzio, M. (2011). Direct visualization at the single-cell level of siRNA electrotransfer into cancer cells. *Proc. Natl. Acad. Sci. U.S.A.* **108**, 10443-10447.

Perea-Gomez, A., Lawson, K. A., Rhinn, M., Zakin, L., Brulet, P., Mazan, S. and Ang, S. L. (2001). Otx2 is required for visceral endoderm movement and for the restriction of posterior signals in the epiblast of the mouse embryo. *Development* **128**, 753-765.

Pucihar, G., Kotnik, T., Valič, B. and Miklavčič, D. (2006). Numerical determination of transmembrane voltage induced on irregularly shaped cells. *Ann. Biomed. Eng.* **34**, 642-652.

Pucihar, G., Miklavcic, D. and Kotnik, T. (2009). A time-dependent numerical model of transmembrane voltage inducement and electroporation of irregularly shaped cells. *IEEE Trans. Biomed. Eng.* **56**, 1491-1501.

Rivera-Pérez, J. A., Mager, J. and Magnuson, T. (2003). Dynamic morphogenetic events characterize the mouse visceral endoderm. *Dev. Biol.* **261**, 470-487.

Rodriguez, T. A., Casey, E. S., Harland, R. M., Smith, J. C. and Beddington, R. S. P. (2001). Distinct enhancer elements control Hex expression during gastrulation and early organogenesis. *Dev. Biol.* **234**, 304-316.

Rols, M.-P. and Teissié, J. (1998). Electropermeabilization of mammalian cells to macromolecules: control by pulse duration. *Biophys. J.* **75**, 1415-1423.

Rols, M.-P., Delteil, C., Golzio, M., Dumond, P., Cros, S. and Teissie, J. (1998). In vivo electrically mediated protein and gene transfer in murine melanoma. *Nat. Biotechnol.* **16**, 168-171.

Rossant, J. and Tam, P. P. L. (2009). Blastocyst lineage formation, early embryonic asymmetries and axis patterning in the mouse. *Development* **136**, 701-713.

Shimamura, K. and Rubenstein, J. L. (1997). Inductive interactions direct early regionalization of the mouse forebrain. *Development* **124**, 2709-2718.

Soares, M. L., Torres-Padilla, M.-E. and Zernicka-Goetz, M. (2008). Bone morphogenetic protein 4 signaling regulates development of the anterior visceral endoderm in the mouse embryo. *Dev. Growth Differ.* **50**, 615-621.

Srinivas, S., Rodriguez, T., Clements, M., Smith, J. C. and Beddington, R. S. P. (2004). Active cell migration drives the unilateral movements of the anterior visceral endoderm. *Development* **131**, 1157-1164.

Sudsiri, J., Wachner, D. and Gimsa, J. (2007). On the temperature dependence of the dielectric membrane properties of human red blood cells. *Bioelectrochemistry* **70**, 134-140.

Swartz, M., Eberhart, J., Mastick, G. S. and Krull, C. E. (2001). Sparking new frontiers: using in vivo electroporation for genetic manipulations. *Dev. Biol.* **233**, 13-21.

Takaoka, K. and Hamada, H. (2012). Cell fate decisions and axis determination in the early mouse embryo. *Development* **139**, 3-14.

Development (2014) 141, 2349-2359 doi:10.1242/dev.106633

Takaoka, K., Yamamoto, M. and Hamada, H. (2011). Origin and role of distal visceral endoderm, a group of cells that determines anterior-posterior polarity of the mouse embryo. *Nat. Cell Biol.* **13**, 743-752.

Tang, J. C., Szikra, T., Kozorovitskiy, Y., Teixiera, M., Sabatini, B. L., Roska, B. and Cepko, C. L. (2013). A nanobody-based system using fluorescent proteins as scaffolds for cell-specific gene manipulation. *Cell* **154**, 928-939.

Teissié, J., Escoffre, J. M., Paganin, A., Chabot, S., Bellard, E., Wasungu, L., Rols, M. P. and Golzio, M. (2012). Drug delivery by electropulsation: recent developments in oncology. *Int. J. Pharm.* **423**, 3-6.

Trichas, G., Joyce, B., Crompton, L. A., Wilkins, V., Clements, M., Tada, M., Rodriguez, T. A. and Srinivas, S. (2011). Nodal dependent differential localisation of dishevelled-2 demarcates regions of differing cell behaviour in the visceral endoderm. *PLoS Biol.* **9**, e1001019.

Trichas, G., Smith, A. M., White, N., Wilkins, V., Watanabe, T., Moore, A., Joyce, B., Sugnaseelan, J., Rodriguez, T. A., Kay, D. et al. (2012). Multi-cellular rosettes in the mouse visceral endoderm facilitate the ordered migration of anterior visceral endoderm cells. *PLoS Biol.* **10**, e1001256.

Valic, B., Golzio, M., Pavlin, M., Schatz, A., Faurie, C., Gabriel, B., Teissié, J., Rols, M.-P. and Miklavcic, D. (2003). Effect of electric field induced transmembrane potential on spheroidal cells: theory and experiment. *Eur. Biophys. J.* **32**, 519-528.

Viotti, M., Niu, L., Shi, S.-H. and Hadjantonakis, A.-K. (2012). Role of the gut endoderm in relaying left-right patterning in mice. *PLoS Biol.* **10**, e1001276.

Voiculescu, O., Papanayotou, C. and Stern, C. D. (2008). Spatially and temporally controlled electroporation of early chick embryos. *Nat. Protoc.* **3**, 419-426.

Wada, Y., Sun-Wada, G.-H. and Kawamura, N. (2013). Microautophagy in the visceral endoderm is essential for mouse early development. *Autophagy* **9**, 252-254.

Wang, S. and Lee, L. J. (2013). Micro-/nanofluidics based cell electroporation. *Biomicrofluidics* **7**, 11301.

Wang, M., Orwar, O., Olofsson, J. and Weber, S. G. (2010). Single-cell electroporation. *Anal. Bioanal. Chem.* **397**, 3235-3248.

Weaver, M., Dunn, N. R. and Hogan, B. L. (2000). Bmp4 and Fgf10 play opposing roles during lung bud morphogenesis. *Development* **127**, 2695-2704.

Yamamoto, M., Saijoh, Y., Perea-Gomez, A., Shawlot, W., Behringer, R. R., Ang, S.-L., Hamada, H. and Meno, C. (2004). Nodal antagonists regulate formation of the anteroposterior axis of the mouse embryo. *Nature* **428**, 387-392.

Yin, T. and Wu, Y. I. (2013). Guiding lights: recent developments in optogenetic control of biochemical signals. *Pflugers Arch.* **465**, 397-408.